

Comparing supernova remnants around strongly magnetized and canonical pulsars

J. Martin¹, N. Rea^{1,2}, D. F. Torres^{1,3} & A. Papitto¹

¹ *Institute of Space Sciences (CSIC–IEEC), Campus UAB, Faculty of Science, Torre C5-parell, E-08193 Barcelona, Spain*

² *Anton Pannekoek Institute for Astronomy, University of Amsterdam, Postbus 94249, NL-1090-GE Amsterdam, The Netherlands*

³ *Institució Catalana de Recerca i Estudis Avançats (ICREA), 08010 Barcelona, Spain*

ABSTRACT

The origin of the strong magnetic fields measured in magnetars is one of the main uncertainties in the neutron star field. On the other hand, the recent discovery of a large number of such strongly magnetized neutron stars, is calling for more investigation on their formation. The first proposed model for the formation of such strong magnetic fields in magnetars was through alpha-dynamo effects on the rapidly rotating core of a massive star. Other scenarios involve highly magnetic massive progenitors that conserve their strong magnetic moment into the core after the explosion, or a common envelope phase of a massive binary system. In this work, we do a complete re-analysis of the archival X-ray emission of the Supernova Remnants (SNR) surrounding magnetars, and compare our results with all other bright X-ray emitting SNRs, which are associated with Compact Central Objects (CCOs; which are proposed to have magnetar-like B-fields buried in the crust by strong accretion soon after their formation), high-B pulsars and normal pulsars. We find that emission lines in SNRs hosting highly magnetic neutron stars do not differ significantly in elements or ionization state from those observed in other SNRs, neither averaging on the whole remnants, nor studying different parts of their total spatial extent. Furthermore, we find no significant evidence that the total X-ray luminosities of SNRs hosting magnetars, are on average larger than that of typical young X-ray SNRs. Although biased by a small number of objects, we found that for a similar age, there is the same percentage of magnetars showing a detectable SNR than for the normal pulsar population.

1 INTRODUCTION

Supernova explosions are among the most energetic and extreme events ever observed in the Universe. Supernovae are mainly distinguished in two main classes: core-collapse (CC) and thermonuclear supernovae. Core-collapse SNe result from the core collapse of a massive star ($> 8 M_{\odot}$; see Woosley & Janka 2005, for a review), while thermonuclear SNe are due to the explosion of a white dwarf in a binary system with a giant star (single-degenerate origin), or from two low-mass white dwarfs in a binary system (double-degenerate origin; Hillebrandt & Niemeyer 2000). Core-collapse SNe might leave behind a fast rotating (several milliseconds) and strongly magnetized ($> 10^{12}$ G) stellar core which is now made by degenerate matter: a so-called neutron star. At the same time the envelope of the massive star, ejected at high speed ($\sim 10^4 \text{ km s}^{-1}$) into the interstellar medium, interacts with it, resulting in what is called a Supernova Remnant (SNR). In the standard picture a SNR evolves in time following four main expansion phases: free expansion, Sedov-Taylor phase, radiative and merging phase. The timescales and properties of each of those phases are characterized by the initial SN explosion energy, inter-

stellar ambient density, and the age of the remnant (see Vink 2012 for a recent review).

In the recent years, a class of highly magnetized neutron stars (a.k.a. magnetars) have been discovered. Magnetars are a small group of X-ray pulsars (about twenty objects with spin periods between 2–12 s) the emission of which is not explained by the common scenario for pulsars. In fact, the very strong X-ray emission of these objects ($L_x \sim 10^{35}$ erg) seemed too high and variable to be fed by the rotational energy alone (as in the radio pulsars), and no evidence for a companion star has been found in favor of any accretion process (see Mereghetti 2008 and Rea & Esposito 2011 for reviews). Assuming the typical magnetic loss equation for rotating neutron stars, their inferred magnetic fields appear to be in general of the order of $B \sim 10^{14} - 10^{15}$ G (although low magnetic field magnetars have been recently discovered Rea et al. 2010, 2012). Because of these high B fields, the emission of magnetars is thought to be powered by the decay and the instability of their strong fields (Duncan & Thompson 1992; Thompson & Duncan 1993; Thompson et al. 2002).

The exact mechanism playing a key role in the formation of such strong magnetic fields is currently debated; in

particular it is not clear which are the characteristics of a massive star turning into a “magnetar” instead of a normal radio pulsar, after its supernova explosion.

Preliminary calculations have shown that the effects of a turbulent dynamo amplification occurring in a newly born neutron star can indeed result in a magnetic field of a few 10^{17} G. This dynamo effect is expected to operate only in the first ~ 10 s after the supernova explosion of the massive progenitor, and if the proto-neutron star is born with sufficiently small rotational periods (of the order of a few ms). The resulting amplified magnetic fields are expected to have a strong multipolar structure, and toroidal component (Duncan & Thompson 1992, 1996; Thompson & Duncan 1993). However, this scenario is encountering more and more difficulties: i) if magnetic torques can indeed remove angular momentum from the core via the coupling to the atmosphere in a pre-SN phase, then the core soon after the SN might not spin rapidly enough for this convective dynamo mechanism to take place (Heger et al. 2005); ii) such a fast spinning proto-neutron star would require a supernova explosion one order of magnitude more energetic than normal supernovae, possibly an hypernova, which is not yet clear on whether it can indeed form a neutron star instead of a black hole. Recent simulations have shown that gamma-ray bursts (GRBs) and hyper-luminous supernovae can indeed be powered by recently formed millisecond magnetars (Metzger et al. 2011; Bucciantini et al. 2012), although no observational evidence of the existence of such fast spinning and strongly magnetized neutron stars have been collected thus far.

Besides the fast spinning proto-neutron star, a further idea on the origin of these high magnetic fields is that they simply reflect the high magnetic field of their progenitor stars. Magnetic flux conservation (Woltjer 1964) implies that magnetars must then be the stellar remnants of stars with internal magnetic fields of $B > 1$ kG, whereas normal radio pulsars must be the end products of less magnetic massive stars.

Recent theoretical studies showed that there is a wide spread in white dwarf progenitor magnetic fields (Wickramasinghe & Ferrario 2005), which, when extrapolated to the more massive progenitors implies a similar wide spread in neutron stars progenitors (Ferrario & Wickramasinghe 2006). Hence, apparently it seems that a fossil magnetic field might be the solution of the origin of such strongly magnetized neutron stars, without the need of invoking dynamo actions on utterly fast spinning proto-neutron stars.

However, this lead to the problem of the formation of such high B progenitor stars. The most common idea is that the magnetic field in the star reflects the magnetic field of the cloud from which the star is formed. The best studied very massive stars (around $\sim 40 M_{\odot}$) with a directly measured magnetic field are θ Orion C and HD191612, with dipolar magnetic field of 1.1 kG and 1.5 kG, respectively (Donati et al. 2002, 2006). Very interestingly, the magnetic fluxes of both these stars (1.1×10^{27} G cm² for θ Orion C and 7.5×10^{27} G cm² for HD191612) are comparable to the flux of the highest field magnetar SGR 1806-20 (5.7×10^{27} G cm²; Woods & Thompson 2006). Other high magnetic field stars are reported in Oskinova et al. (2011).

Recent observations of the environment of some magne-

| SNR | Instrument | ObsID | Date | Detector | Exp. (s) | |
|--------------|----------------|------------|------------|------------|----------|-------|
| Kes73 | XMM | 0013340101 | 2002-10-05 | PN | 6017 | |
| | | | | MOS1 | 5773 | |
| | | | | MOS2 | 5771 | |
| CTB 109 | XMM | 0013340201 | 2002-10-07 | PN | 6613 | |
| | | | | MOS1 | 6372 | |
| | | | | MOS2 | 6372 | |
| | | 0057540101 | 2002-01-22 | PN | 12237 | |
| | | | | MOS1 | 19027 | |
| | | | | MOS2 | 19026 | |
| N49 Kes75 | XMM Chandra | 0057540201 | 2002-07-09 | PN | 14298 | |
| | | | | MOS1 | 17679 | |
| | | | | MOS2 | 17679 | |
| | | 0057540301 | 2002-07-09 | PN | 14011 | |
| | | | | MOS1 | 17379 | |
| | | | | MOS2 | 17379 | |
| N49 Kes75 | XMM Chandra | 0505310101 | 2007-11-10 | PN | 72172 | |
| | | | | 2000-10-15 | ACIS-S | 37280 |
| | | | | | ACIS-S | 54070 |
| | | | | | ACIS-S | 17360 |
| | | | | | ACIS-S | 39250 |
| 2006-06-12 | ACIS-S | 44110 | | | | |

Table 1. Observations used in this paper.

tars revealed strong evidence that these objects are formed from the explosion of very massive progenitors ($M > 30 M_{\odot}$). In particular: i) a shell of HI has been detected around 1E 1048.1–5937, and interpreted as ISM displaced by the wind of a progenitor of 30–40 M_{\odot} (Gaensler et al. 2005); SGR 1806–20 and SGR 1900+14 have been claimed to be hosted by very young and massive star clusters, providing a limit on their progenitor mass of $> 50 M_{\odot}$ (Fuchs et al. 1999; Figer et al. 2005; Davies et al. 2009) and $> 20 M_{\odot}$ (Vrba et al. 2000), respectively. Finally, CXOU 010043-7211 is a member of the massive cluster Westerlund 1 (Muno et al. 2006; Ritchie et al. 2010), with a progenitor with mass estimated to be $> 40 M_{\odot}$ (see also Clark et al. 2014).

Vink & Kuiper (2006) have started the idea of studying the energetics of supernova remnants surrounding magnetar with the aim of disentangling a possible energetic difference between those remnants and others surrounding normal pulsars. Their work did not find any clear evidence i.e. of an additional energy released in the remnant possibly due to an excess of rotational energy at birth.

Following this study we decided to extend their work re-analyzing all available *XMM-Newton* or *Chandra* data of all confirmed and bright SNRs associated with a magnetar or with a high-B pulsar showing magnetar-like activity, and comparing in a coherent and comprehensive way all the extracted properties of these SNRs with other remnants: in particular line ionization and X-ray luminosity. In section §2 we report on the data analysis and reduction of our observational sample, in §3 the results of our analysis, and we discuss our findings in §4.

2 DATA ANALYSIS AND REDUCTION

In this work, our approach has tried to be as conservative and model independent as possible. In particular, our target sample has been chosen such to include all confirmed associations (see the McGill catalog¹ for all proposed associations), and among those, we chose only those supernova remnants bright enough, and with sufficiently good spectra, to perform a detailed analysis and classification of their spectral lines. We analyze the X-ray spectral lines of four SNRs

¹ <http://www.physics.mcgill.ca/pulsar/magnetar/main.html>

hosting a neutron star that showed magnetar-like activity in its center: Kes 73, CTB 109, N 49 and Kes 75. We use for all targets the best available archival data: from the *XMM-Newton* telescope in the case of Kes 73, CTB 109 and N 49, and *Chandra* for Kes 75. The observations used are summarized in Table 1. To compare coherently all the spectral lines and fluxes we observed for these remnants we have chosen to use an empirical spectral fitting for all SNRs. We have modeled all spectra using one or two Bremsstrahlung models for the spectral continuum, plus Gaussian functions for each detected spectral line. We added spectral lines one by one until the addition of a further line did not significantly improve the fit (by using the F-test). This approach is totally empirical, with respect of using more detailed ionized plasma models, but ensures a coherent comparison between different remnants. In Table 5, we report also the results of our spectra modeled with ionized plasma models, for a comparison with the literature.

2.1 *XMM-Newton* data

We use images in full-frame mode obtained from the European Photon Imaging Camera (EPIC) PN (Strüder et al. 2001) and MOS (Turner et al. 2001). The spectra of these images are fitted simultaneously in order to obtain the spectrum with the maximum possible number of counts. We used the specific software for *XMM-Newton* data, Science Analysis System (SAS) v13.5.0 with the latest calibration files. To clean images of solar flares, we used the SAS tool *tabtigen* to choose the good time intervals and extract them and the spectra with *evselect*. Source and background spectra were extracted from each single image with pattern ≤ 4 for PN images and pattern ≤ 12 for MOS. The spectra and the backgrounds corresponding to the same regions and the same detector were merged using the FTOOLS routine *mathpha* and we compute the mean of the response matrices (RMF) and the ancillary files (ARF) weighted by the exposure time using the tools *addrmf* and *addarf* (this means, that we keep PN, MOS1 and MOS2 data separately and we merge the spectra when they come from the same detector). Finally, we binned the spectra demanding a minimum of 25 counts per bin to allow the use of χ^2 -statistics.

We analyze the spectrum of each nebula considering its entire extension. For Kes 73, the nebula is completely covered in the EPIC PN, MOS 1 and MOS 2 detectors and we consider all of them in the analysis. In the case of CTB 109, the SNR is too large to be included entirely in a single pointing. The images with the *XMM-Newton* data ID: 0057540101, 0057540201 and 0057540301 correspond to south, north and east pointings of the remnant. We computed the spectra of each pointing, also considered the EPIC PN, MOS 1 and MOS 2 cameras. For N 49, the exposure time of the MOS detectors is very low in comparison with PN. For this reason, we did not use the MOS data to avoid statistical noise in the data.

2.2 *Chandra* data

In the case of Kes 75, the best available observations were performed with *Chandra* using the Advanced CCD Imaging Spectrometer (ACIS). The ID numbers of the data used

are in Table 1. We used the standard reduction software for *Chandra*, the Chandra Interactive Analysis of Observations (CIAO) v4.5. The spectra and the backgrounds were extracted using the routine *specextract* and the RMFs and ARFs using *mkacisrmf* and *mkwarf* respectively. Finally, we combine the spectra demanding a minimum of 25 counts per energy bin using *combine_spectra*.

3 SPECTRAL ANALYSIS AND RESULTS

We report the fitted spectra in figure 3, while reporting the best fitting models and relative parameters in Tables 3 and 4. For the spectral analysis, we used the program *XSPEC* (Arnaud 1996) v12.8.1 from the package HEASOFT v6.15. As anticipated above, we have used for all SNRs a spectral model comprised of photo-electric absorption (**phabs**), one or two Bremsstrahlung models (**brems**), plus a series of Gaussian functions to model the emission lines. Even if more physical ionized plasma models such as **vnei**, **vshock** or **vpshock** could be used to fit those SNRs: e. g., Kumar et al. (2014) for Kes 73, Sasaki et al. (2004, 2013) for CTB 109, Park et al. (2012) for N 49 and Temim et al. (2012) for Kes 75; we prefer to use a more empirical approach to compare coherently the emission lines and luminosities of those objects, which is the aim of our work. Below we summarize for each studied remnant our results in the context of the general properties of the SNR.

In Figure 2 we show the background regions we have chosen for this analysis. We have tried several different regions finding consistent results. During the spectral analysis we checked that subtracting the background spectra or fitting it separately from the remnant spectra and subtracting its best fitting model, gave consistent results.

3.1 Kes 73

Kes 73 (also known as G27.4+0.0) is a shell-type SNR. Its dimensions are about $4.7' \times 4.5'$ and it is located between 7.5 and 9.8 kpc (Tian & Leahy 2008b). The central source is the magnetar 1E 1841–045 discovered as a compact X-ray source with the Einstein Observatory (Kriss et al. 1985), and confirmed as a magnetar in Vasisht & Gotthelf (1997); Gotthelf et al. (1999b). The period of the magnetar is 11.78 s and its period derivative is $4.47 \times 10^{-11} \text{ s s}^{-1}$. The resulting dipolar magnetic field is $7.3 \times 10^{14} \text{ G}$, the spin-down luminosity is $1.1 \times 10^{33} \text{ erg s}^{-1}$ and the characteristic age is 4180 yr. The age of the SNR shell is estimated around 1300 yr (Vink & Kuiper 2006), which is consistent with the age between 750 and 2100 yr estimated by Kumar et al. (2014). Kes 73 has been also observed by *ROSAT* (Helfand et al. 1994), *ASCA* (Gotthelf & Vasisht 1997), *Chandra* (Lopez et al. 2011) and *Suzaku* (Sezer et al. 2010).

Kes 73 shows a quite spherical structure with 1E 1841-045 in the center of the remnant (see Figure 1). In the western part of the nebula (right-hand side of the images), we distinguish a shock ring which encloses the central source from west to east of the image passing below the central source. Most of the flux is emitted between 1 and 3 keV. Finally, we analyzed the total spectrum of the nebula excluding a circle of $40''$ around the central source to exclude

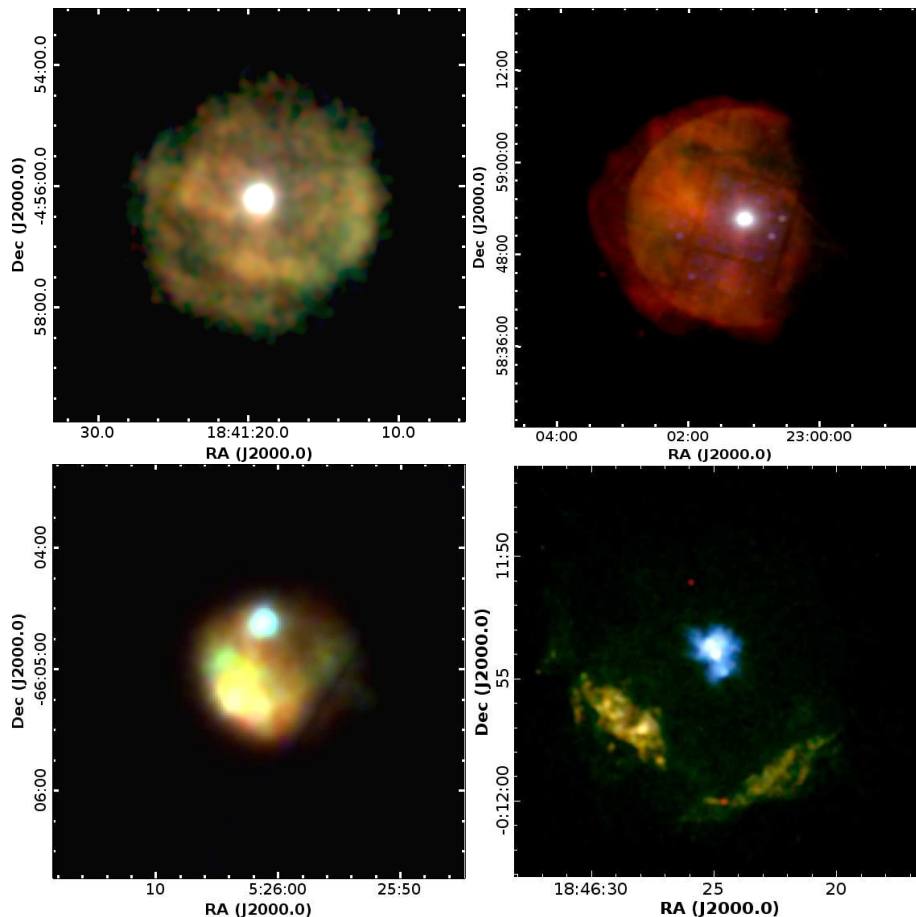


Figure 1. Combined color images of Kes 73 (top-left), CTB 109 (top-right), N49 (bottom-left) and Kes 75 (bottom-right).

possible contamination from the central object. The background spectrum has been extracted from a surrounding annular region shown in Figure 2, avoiding gaps between the CCDs to ensure good convergence of the response matrices. The continuum spectrum has been fitted with two plasmas with temperatures of 0.43 keV and 1.34 keV. The absorption column density obtained is $N_{\text{H}} = 2 \times 10^{22} \text{ cm}^{-2}$. We detected 6 lines. The most prominent is the Fe XXV at 6.7 keV with an equivalent width (EW) of 1.89 keV. Other lines are Mg XI at 1.35 keV (EW=95 eV), Si XIII at 1.85 keV (EW=0.37 keV), Si XIII at 2.19 keV (EW=46 eV), S XV at 2.45 keV (EW=0.38 keV) and Ar XVII at 3.13 keV (EW=0.12 keV).

3.2 CTB 109

CTB 109 (also G109.2-1.0) was discovered in X-rays with the Einstein Observatory by Gregory & Fahlman (1980), it is $30' \times 45'$ wide and the estimated distance is about 3 kpc (Kothes et al. 2002). The central source is the magnetar 1E 2259+586 with a spin period of 6.98 s (Fahlman & Gregory 1983) and a period derivative of 4.83×10^{-13} (Iwasawa et al. 1992). The dipolar magnetic field is about 5.9×10^{13} G, the spin down power is $5.6 \times 10^{31} \text{ erg s}^{-1}$ and the characteristic age is 229 kyr. Despite the large characteristic age of the pulsar, the estimated true age of the remnant is about 14 kyr (Sasaki et al. 2013). CTB 109 has been observed also in X-rays with *ASCA* (Rho et al. 1998), *Bep-*

poSAX (Parmar et al. 1998) and *ROSAT* (Hurford & Fesen 1995; Rho & Petre 1997).

The spectrum covers the entire shell and combines the three observations detailed in Table 1. The background regions used are shown in Figure 2. We observe that the main contribution to the flux is in the energy range between 0.5 and 2 keV. Some known X-ray sources in the field of view have been excluded in our analysis.

In this case we used two Bremsstrahlung models to fit the continuum, with temperatures of 0.07 keV and 0.20 keV. The measured absorption density is $N_{\text{H}} = 2.83 \times 10^{22} \text{ cm}^{-2}$, and we detected 6 lines: N VII at 0.52 keV (EW=0.74 keV) and at 0.60 keV (EW=0.47 keV), Ne IX at 0.91 keV (EW=0.15 keV), Ne X at 1.01 keV (EW=68 eV), Mg XI at 1.35 keV (EW=0.34 keV) and Si XIII at 1.86 keV (0.28 keV).

3.3 N 49

N49 (also SNR B0525-66.1) is a SNR located in the Large Magellanic Cloud (LMC). The associated central source is SGR 0526-66 with a period of 8.047 s (Mazets et al. 1979) and a period derivative of $6.6 \times 10^{-11} \text{ s s}^{-1}$ (Kulkarni et al. 2003). There is some uncertainty in the association of SGR 0526-66 with N49 (see Gaensler et al. 2001). The inferred dipolar magnetic field is 7.3×10^{14} G, the spin-down luminosity is $4.9 \times 10^{33} \text{ erg/s}$ and the characteristic age is ~ 2

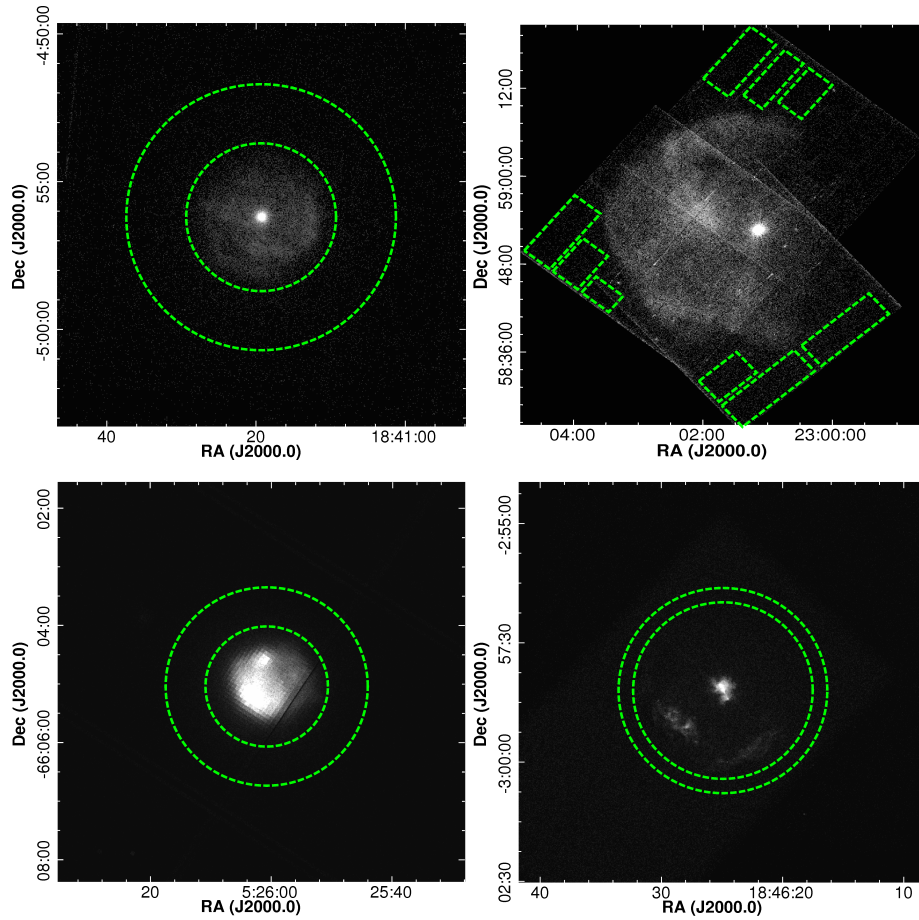


Figure 2. Map of the backgrounds used in the spectrum analysis. The order of the images is the same as in figure 1.

kyr. The nebula is $1.5' \times 1.5'$, this means that assuming a distance of 50 kpc the diameter of N49 is ~ 22 pc. Park et al. (2012) establish a Sedov age for the nebula of ~ 4.8 kyr and a SN explosion energy of 1.8×10^{51} erg.

SGR 0526-66 is located in the north of the remnant. The brightest part of the nebula is in the southeast, coinciding with dense interstellar clouds (Vancura et al. 1992; Banas et al. 1997; Park et al. 2012). This part of the remnant also has contributions between 3 and 10 keV, while the contribution of the rest of the nebula is clearly negligible at this range. In Figure 1, we show a color image of N49. We analyze the total spectrum of the nebula excluding a circle of $20''$ around the central source to avoid its contribution to the spectrum.

The absorption of N49 has two components: one is related with the Galactic absorption and the other is the absorption produced by LMC. The Milky Way photoelectric absorption towards N49 is fixed as $N_{\text{H}} = 6 \times 10^{20} \text{ cm}^{-2}$ (Dickey & Lockman 1990; Park et al. 2012). We include a second absorption component to take into account the absorption column density for LMC, where we use the abundances given by Russell & Dopita (1992); Hughes et al. (1998); Park et al. (2012). We obtain an absorption column density of $N_{\text{H}} = 0.7 \times 10^{22} \text{ cm}^{-2}$ for the LMC contribution. The continuum is represented by two Bremsstrahlung models with temperatures of 0.23 keV and 1.14 keV. In this case, we have detected 9 lines: O VII at 0.57 keV (EW=0.20 keV),

O VIII/Fe XVIII at 0.77 keV (EW=0.34 keV), Ne X at 1.03 keV (EW=33 eV), Mg XI at 1.33 keV (EW=62 eV), Mg XII at 1.46 keV (EW=20 eV), Si XIII at 1.85 keV (EW=0.30 keV), Si XIV at 2.00 keV (EW=0.13 keV), S XV at 2.44 keV (EW=0.30 keV) and Ar XVII at 3.12 keV (EW=0.11 keV).

3.4 Kes 75

Kes 75 (G29.7-0.3) is a composite SNR. The X-ray emission of the partial shell is extended in two clouds in the southwest and southeast part of the image (see Figure 1). It was observed firstly in X-rays by *Einstein* (Becker et al. 1983) showing an incomplete shell of $3'$ in extent. In the center of the nebula, there is a bright pulsar wind nebula (PWN), which was spatially resolved by the *Chandra* observation (Helfand et al. 2003; Ng et al. 2008), and PSR J1846-0258 powers it. This pulsar was discovered using the *RXTE* telescope and localized within an arc minute of the remnant using *ASCA* (Gotthelf et al. 2000). The period of the pulsar is ~ 326 ms and the period derivative $7.11 \times 10^{-12} \text{ s s}^{-1}$ (e.g., Livingstone et al. 2011a). This leads to a spin-down energy loss of $8.1 \times 10^{36} \text{ erg s}^{-1}$, a magnetic field of 4.9×10^{13} G and a characteristic age of 728 yr. Livingstone et al. (2006) estimated a braking index of 2.65 ± 0.01 . Despite its early classification as a typical rotational powered pulsar, PSR J1846-0258 showed magnetar-like activity via short bursts

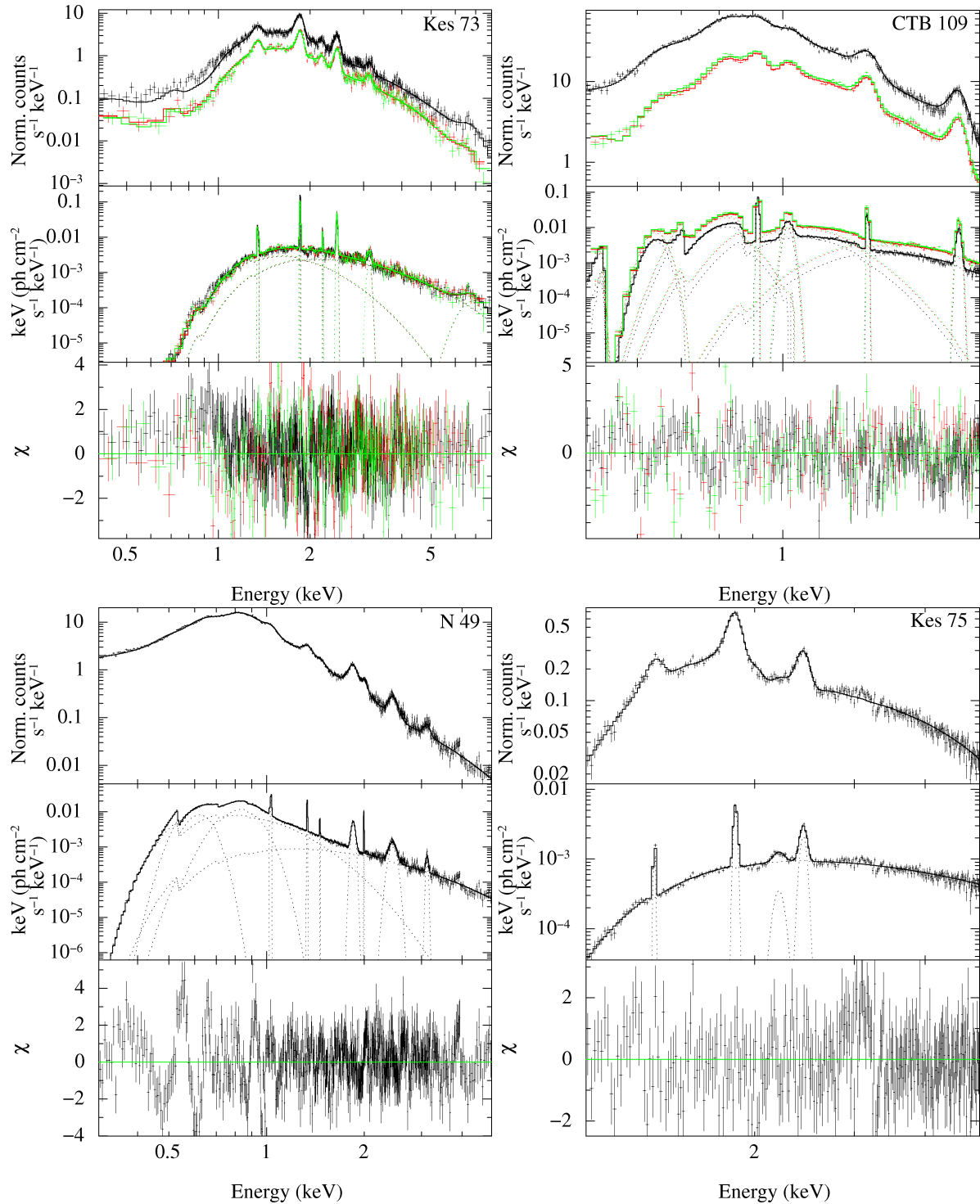


Figure 3. Spectra obtained for the Kes 73, CTB 109, N 49 & Kes 75. We used the EPIC PN (in black), MOS 1 (in red) and MOS 2 (in green) data simultaneously to fit the models.

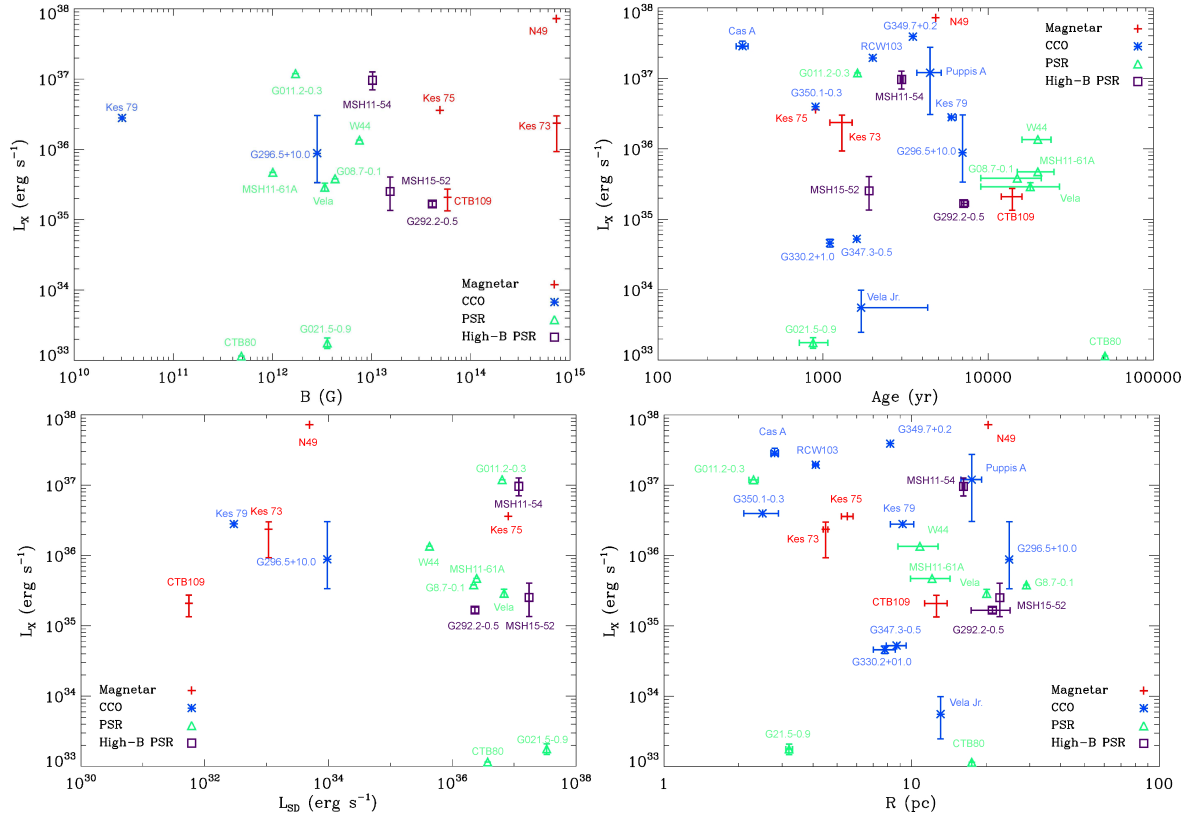


Figure 4. X-ray luminosity of all observed, and securely associated, X-ray emitting SNRs containing a magnetar, a CCO, a high-B pulsar or a normal pulsar, plotted versus magnetic-field (top-left), age (top-right), spin-down luminosity (bottom-left) and remnant radius (bottom-right).

and the outburst of its persistent emission (Gavril et al. 2008; Kumar & Safi-Harb 2008) enabling its classification as (at least sporadically) a magnetically powered pulsar. There is a big uncertainty in the distance of this SNR in the literature (Caswell et al. 1975; Milne 1979; McBride et al. 2008; Becker & Helfand 1984). Most recent estimates give a distance between ~ 5.1 - 7.5 kpc based on H I absorption observations (Leahy & Tian 2008), and 10.6 kpc using millimeter observations of CO lines from an adjacent molecular cloud (Su et al. 2009). In our work, we adopt this value in order to compute the X-ray luminosity and the size of the SNR.

The spectrum of Kes 75 has been fitted using only one thermal Bremsstrahlung component with a temperature of 2.8 keV and an absorption column density of $1.79 \times 10^{22} \text{ cm}^{-2}$. Four clear lines are resolved using Gaussians: Mg XI line at 1.33 keV (EW=84 eV), two Si XIII lines at 1.85 (EW=0.23 keV) and 2.21 keV (EW=45 eV) and S XV at 2.44 keV (EW=0.18 keV).

4 DISCUSSION

In this work we have re-analyzed in a coherent way the X-ray emission from SNRs around magnetars, and compared their emission lines and luminosities. The aim of this study was to search for any possible trend or significant difference in SNRs associated with different types of neutron stars. This work complements and extends the work by Vink & Kuiper (2006), providing a detailed description of the spectra for

Kes 73, Kes 75, N 49 and CTB 109, and compares them directly with other remnants with similar spectroscopic X-ray studies. We also looked for any possible trend or significant difference in the ionization state and X-ray luminosity of SNRs associated with different types of neutron stars.

4.1 Spectral lines comparison with other SNRs

X-ray spectra of SNRs are usually fit with plasma models (see also Table 5). In this work we proceed to fit the spectra of Kes 73, CTB 109, N 49 and Kes 75 using a thermal Bremsstrahlung model for the continuum emission and Gaussians for the lines. Our main aim is to have an estimate of line centroid energy, to identify it properly. We have then used the simplest continuum model to reduce the free parameters of the fit². One could expect that the excess of rotational energy released by the magnetar during the alpha-dynamo process could be stored in the ionization level of the lines present in the spectrum. If the energy release is higher than in a normal SNR, heavy elements such as silicon (Si), sulfur (S), argon (Ar), calcium (Ca) or iron (Fe) could be systematically at a higher state of ionization. In Table 3, we collected all SNRs with detailed spectroscopic studies in the literature and we see that the typical elements detected are O VII, O VIII, Ne IX, Ne X, Mg XI, Mg XII, Si XIII, Si

² Note that in the 0.5-1 keV the detection of spectral lines are dependent on absorption model we adopted.

XIV, S XV, S XVI, Ar XVII, Ca XIX and Fe XXV. The only lines detected in all four of the spectra are the Mg XI line at 1.33 keV and Si XIII at 1.85 keV. For comparison, we also fitted the spectra of the SNRs using a `vnei` model (e. g., Borkowski et al. 2001). The results are summarized in the Table 5. We have added a thermal Bremsstrahlung component in some cases. The temperature of the `vnei` plasma is always higher than for the thermal Bremsstrahlung, with the exception of N49 in which the temperature for `vnei` is 0.17 keV (0.99 keV for Bremsstrahlung). The abundances obtained in both models show similar tendencies. For Kes 73 and N 49, the abundances of Si and S are quite above the solar ones. CTB 109 shows low abundances with respect to the solar ones for O, Ne, Mg, Si and Fe. Due to the complexity of the N 49 spectrum, some lines have not been reproduced well by the plasma models and we have added them using gaussian profiles to improve the fit. In summary, our spectroscopic X-ray analysis of these sources shows compatible results with other non-magnetar SNRs already reported in literature.

4.2 Comparison with other SNRs

In Figure 4 we have collected from the literature the X-ray luminosities from 0.5 to 10 keV of all observed SNRs brighter than $\sim 10^{33}$ erg s $^{-1}$, with an age lower than 100 kyr and having a confirmed association with a central source. For these remnants, we obtain the age, distance, approximate radius, magnetic field and spin-down luminosity of the central source (whenever possible) from the literature. All this information is summarized in Table 6. We have plotted the SNRs luminosities (excluding the contribution of the central neutron star luminosity) as a function of the SNR age and dimension (although note that the latter parameter is highly dependent on the environment of each remnant). For those remnants having a central neutron star with measured rotational properties, we plot the SNR luminosity as a function of the pulsar surface dipolar magnetic field at the equator ($B = 3.2 \times 10^{19} \sqrt{P\dot{P}}$ G), and the pulsar spin down luminosity ($L_{sd} = 3.9 \times 10^{46} \dot{P}/P^3$ erg/s; always assuming the neutron star moment of inertia $I = 10^{45}$ g cm 2), and where P is the pulsar rotation period in seconds and \dot{P} its first derivative.

In order to search for any correlations in the SNRs and pulsars characteristics (see Figure 4), we run a Spearman test. We searched for correlations between the X-ray luminosity and other features of the sources of our sample, such as dimension of the remnant, age, surface magnetic field strength and spin down power of the associated pulsar. To this end, we employed a Spearman rank correlation test, and evaluated the significance of the value of the coefficient of correlation r obtained, by computing $t = r\sqrt{(N-2)/(1-r^2)}$, which is distributed approximately as Student's distribution with $N-2$ degrees of freedom, where N is the number of couples considered. The results we obtained are listed in Table 2; no correlation is found at a significance level larger than 99%, or any significant difference in luminosity between SNRs surrounding magnetars and those around other classes of isolated neutron stars.

We have also been looking at the number of pulsars having detected SNRs as a function of age, and compared

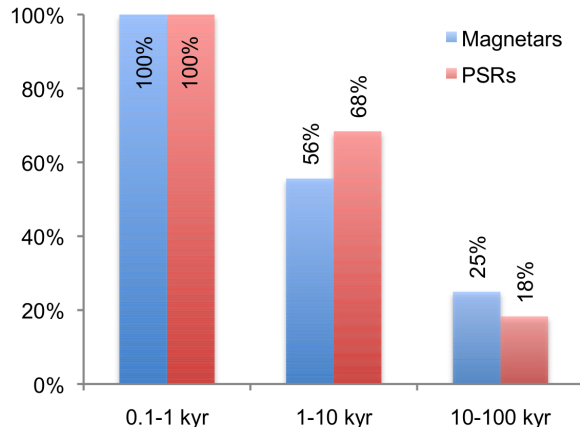


Figure 5. Percentage of pulsars and magnetars having a detected SNR as a function of the age.

| Parameters | r | N | p |
|--------------------|--------|-----|------|
| L_X vs. age | -0.158 | 24 | 0.46 |
| L_X vs. radius | -0.245 | 24 | 0.25 |
| L_X vs. B | 0.271 | 16 | 0.31 |
| L_X vs. L_{sd} | -0.309 | 16 | 0.25 |

Table 2. Spearman correlation coefficient (r), number of couples considered (N) and probability that the two samples are not correlated (p) evaluated by comparing the X-ray luminosity of the sources of our sample with the age, radius, surface magnetic field strength and spin down luminosity.

it to the magnetar case. We caution, however, that there are several systematic effects in this comparison (different detection wavebands, distance, low number of magnetars in comparison with pulsars, etc.), but we were mostly interested in looking for a general trend. In Figure 5 we plot the result of this comparison, where we can see how on average (with all the due caveats) for a similar age, pulsars and magnetars seem to show a similar probability to have a detected SNR.

5 CONCLUSIONS

We have reported on the re-analysis of the X-ray emission of SNRs surrounding magnetars, using an empirical modeling of their spectrum with a Bremsstrahlung continuum plus several emission lines modeled by Gaussian functions. Our analysis, and the comparison of the emission of those remnants with other bright SNR surrounding normal pulsars suggest the following conclusions:

- We find no evidence of generally enhanced ionization states in the elements observed in magnetars' SNRs compared to remnants observed around lower magnetic pulsars.
- No significant correlation is observed between the SNRs X-ray luminosities and the pulsar magnetic fields.
- We show evidence that the percentage of magnetars and pulsars hosted in a detectable SNR are very similar, at a similar age.

Our findings do not support the claim of magnetars being formed via more energetic supernovae, or having a large rotational energy budget at birth that is released in the surrounding medium in the first phases of the magnetar formation. However, we note that although we do not find any hint in the SNRs to support such an idea, we cannot exclude that: 1) most of the rotational energy has been emitted via neutrinos or gravitational waves, hence with no interaction with the remnant; or 2) we are restricted to a very small sample, and with larger statistics some correlation might be observed in the future.

This work was supported by grants AYA2012-39303, SGR2009-811, iLINK 2011-0303 and the NewCOMPSTAR MP1304 COST Action. NR is supported by a Ramón y Cajal fellowship and by an NWO Vidi Award. AP is supported by a Juan de la Cierva fellowship. We are indebted to Samar Safi-Harb and Harsha Kumar for providing the *Chandra* data on Kes 75, and for useful comments. We also thank Manami Sasaki and the referee for comments and suggestions that improved the manuscript.

REFERENCES

- Aharonian, F. et al. 2007, *ApJ*, 661, 236
 Archibald, R. F. et al. 2013, *Nature*, 497, 591
 Arnaud, K. A. 1996, *ASP Conf. Ser.*, 101, *Astronomical Data Analysis and Systems V*, ed. G. Jacoby & J. Barnes (San Francisco: ASP), 17
 Aschenbach, B., Egger, R. & Trümper, J. 1995, *Nature*, 373, 587
 Banas, K. R., Hughes, J. P., Bronfman, L. & Nyman, L. 1997, *ApJ*, 480, 607
 Becker, R. H., Helfand, D. J. & Szymkowiak, A. E. 1983, *ApJ*, 268, L93
 Becker, R. H. & Helfand, D. J. 1984, *ApJ*, 283, 154
 Becker, W., Prinz, T., Winkler, P. F. & Petre, R. 2012, *ApJ*, 755, 141
 Bietenholz, M. F. & Bartel, N. 2008, *MNRAS*, 386, 1411
 Blanton, E. L. & Helfand, D. J. 1996, *ApJ*, 470, 961
 Bleeker, J. A. et al. 2001, *A&A*, 365, L225
 Borkowski, K. J., Lyster, W. J. & Reynolds, S. P. 2001, *ApJ*, 548, 820
 Borkowski, K. J. et al. 2010, *ApJL*, 724, L161
 Bucciantini, N., Metzger, B. D., Thompson, T. A. & Quataert, E. 2012, *MNRAS*, 419, 1537
 Carter, L. M., Dickel, J. R. & Bomans, D. J. 1997, *PASP*, 109, 990
 Case, G. L. & Bhattacharya, D. 1998, *ApJ*, 504, 761
 Cassam-Chenaï, G. et al. 2004, *A&A*, 414, 545
 Caswell, J. L., Murray, J. D., Roger, R. S., Cole, D. J. & Cooke, D. J. 1975, *A&A*, 45, 239
 Caswell, J. L., McClure-Griffiths, N. M. & Cheung, M. C. M. 2004, *MNRAS*, 352, 1405
 Clark, J. S., Ritchie, B. W., Najarro, F., Langer, N. & Negueruela, I. 2014, *A&A*, 565, 90
 Cox, D. P. et al. 1999, *ApJ*, 524, 179
 Davies, B. et al. 2009, *ApJ*, 707, 844
 Decourchelle, A. et al. 2001, *A&A*, 365, L218
 Dickey, J. M. & Lockman, F. J. 1990, *ARA&A*, 28, 215
 Dodson, R. G., McCulloch, P. M. & Lewis, D. R. 2002, *ApJ*, 564, L85
 Dodson, R. G., Legge, D., Reynolds, J. E. & McCulloch, P. M. 2003, *ApJ*, 596, 1137
 Donati, J. F., Babel, J., Harries, T. J., Howarth, I. D., Petit, P. & Semel, M. 2002, *MNRAS*, 333, 55
 Donati, J. F., Howarth, I. D., Bouret, J. C., Petit, P., Catala, C. & Landstreet, J. 2006, *MNRAS*, 365, 6
 Dubner, G. et al. 2013, *A&A*, 555, 9
 Duncan, R. C. & Thompson, C. 1992, *ApJ*, 392, L9
 Duncan, R. C. & Thompson, C. 1996, *AIP conf. proc.*, 366, 111
 Fahlman, G. G. & Gregory, P. C. 1983, *IAU Symp.* 101, *Supernova Remnants and Their X-Ray Emission*, ed. J. danziger & P. Gorenstein (Dordrecht: Kluwer), 445
 Fang, J. & Zhang, L. 2010, *A&A*, 515, 20
 Ferrand, G. & Safi-Harb, S. 2012, *AdSpR*, 49, 1313
 Ferrario, L. & Wickramasinghe, D. 2006, *MNRAS*, 367, 1323
 Fesen, R. A. et al. 2006, *ApJ*, 645, 283
 Fesen, R. A., Kremer, R., Patnaude, D. & Milisavljevic, D. 2012, *AJ*, 143, 27
 Figer, D. F., Najarro, F., Gaballe, T. R., Blum, R. D., & Kudritzki, R. P. 2005, *ApJ*, 622, L49
 Finley, J. P. & Oegelman, H. 1994, *ApJ*, 434, L25
 Frail, D. A. et al. 1996, *AJ*, 111, 1651
 Fuchs, Y., Mirabel, F., Chaty, S., Claret, A., Cesarsky, C. J. & Cesarsky D. A. 1999, *A&A*, 350, 891
 Gaensler, B. M., Brazier, K. T. S., Manchester, R. N., Johnston, S. & Green, A. J. 1999, *MNRAS*, 305, 724
 Gaensler, B. M., Slane P. O., Gotthelf, E. V. & Vasisht, G. 2001, *ApJ*, 486, L133
 Gaensler, B. M. & Wallace, B. J. 2003, *ApJ*, 594, 326
 Gaensler, B. M., McClure-Griffiths, N. M., Oey, M. S., Haverkorn, M., Dickey, J. M. & Green, A. J. 2005, *ApJ*, 620, L95
 Gaensler, B. M. 2008, *ApJ*, 680, L37
 Gavriil, F. P. et al. 2008, *Science*, 319, 1802
 Giacani, E. B., Dubner, G. M., Green, A. J., Goss, W. M. & Gaensler, B. M. 2000, *AJ*, 119, 281
 Gotthelf, E. V. & Vasisht, G. 1997, *ApJ*, 486, L133
 Gotthelf, E. V., Petre, R. & Vasisht, G. 1999, *ApJ*, 514, L107
 Gotthelf, E. V., Vasisht, G. & Dotani T. 1999, *ApJ*, 522, L49
 Gotthelf, E., Vasisht, G., Boylan-Kolchin, M. & Torii, K. 2000, *ApJ*, 542, L37
 Gregory, P. C. & Fahlman, G. G. 1980, *Nat*, 287, 805
 Halpern, J. P. & Gotthelf, E. V. 2010, *ApJ*, 709, 436
 Hayato, A. et al. 2010, *ApJ*, 725, 894
 Heger, A., Woosley, S. E., & Spruit, H. C. 2005, *ApJ*, 626, 350
 Helfand, D. J., Becker, R. H., Hawkins, G. & White, R. L. 1994, *ApJ*, 434, 627
 Helfand, D. J., Collins, B. F. & Gotthelf, E. V. 2003, *ApJ*, 582, 783
 Hillebrandt, W. & Niemeyer, J. C., 2000, *ARA&A*, 38, 191
 Hobbs, G., Lyne, A. G., Kramer, M., Martin, C. E. & Jordan, C. 2004, *MNRAS*, 353, 1311
 Hughes, J. P., Hayashi, I. & Koyama, K. 1998, *ApJ*, 505, 732

- Hughes, J. P., Slane, P. O., Park, S., Roming, P. W. A. & Burrows, D. N. 2003, *ApJ*, 591, L139
- Hurford, A. P. & Fesen, R. A. 1995, *MNRAS*, 277, 549
- Hwang, U. & Gotthelf, E. V. 1997, *ApJ*, 475, 665
- Hwang, U., Petre, R. & Flanagan, K. A. 2008, *ApJ*, 676, 378
- Iwasawa, K., Koyama, K. & Halpern, J. P. 1992, *PASJ*, 44, 9
- Kaspi, V. M. et al. 2001, *ApJ*, 560, 371
- Katsuda, S., Tsunemi, H. & Mori, K. 2008, *ApJ*, 678, L35
- Kellett, B. J. et al. 1987, *MNRAS*, 225, 199
- Kinugasa, K. & Tsunemi, H. 1999, *PASJ*, 51, 239
- Kothes, R., Uyaniker, B. & Yar, A. 2002, *ApJ*, 576, 169
- Koyama, K. et al. 1997, *PASJ*, 49, L7
- Kriss, G. A., Becker, R. H., Helfand, D. J. & Canizares C. R. 1985, *ApJ*, 288, 703
- Kuiper, L., Hermsen, W., den Hartog, P. R. & Collmar, W. 2006, *ApJ*, 645, 556
- Kulkarni, S. R. et al. 2003, *ApJ*, 585, 948
- Kumar, H. S. & Safi-Harb, S. 2008, *ApJ*, 678, 43
- Kumar, H. S., Safi-Harb, S. & Gonzalez, M. E. 2012, *ApJ*, 754, 96
- Kumar, H. S., Safi-Harb, S., Slane, P. O. & Gotthelf, E. V. 2014, *ApJ*, 781, 41
- Lazentic, J. S. et al. 2003, *ApJ*, 593, L27
- Lazentic, J. S., Slane, P. O., Hughes, J. P., Chen, Y. & Dame, T. M. 2005, *ApJ*, 618, 733
- Leahy, D. A. & Tian, W. W. 2008, *A&A*, 480, L25
- Livingstone, M. A., Kaspi, V. M., Gotthelf, E. V. & Kuiper, L., 2006, *Apj*, 647, 1286
- Livingstone, M. A., Ng, C.-Y., Kaspi, V. M., Gavriil, F. P. & Gotthelf, E. V. 2011, *ApJ*, 730, 66
- Livingstone, M. A. & Kaspi, V. M. 2011, *ApJ*, 742, 31
- Lopez, L. A., Ramirez-Ruiz, E., Huppenkothen, D., Badenes, C. & Pooley D. A. 2011, *ApJ*, 732, 114
- Lu, F. J. & Aschenbach, B. 2000, *A&A*, 362, 1083
- Maeda, Y. et al. 2009, *PASJ*, 61, 1217
- Matheson, H. & Safi-Harb, S. 2010, *ApJ*, 724, 572
- Matsui, Y., Long, K. S. & Tuohy, I. R. 1988, *ApJ*, 329, 838
- Mazets, E. P., Golenetskii, S. V., Il'inskii, V. N., Aptekar R. L. & Guryan Y. A. 1979, *Nat*, 282, 587
- McBride, V. A., Dean, A. J. & Bazzano, F. 2008, *A&A*, 477, 249
- Mereghetti, S., Tiengo, A. & Israel, G. L. 2002, *ApJ*, 569, 275
- Mereghetti, S. 2008, *A&ARv*, 15, 225
- Metzger, B. D., Giannios, D., Thompson, T. A., Bucciantini, N. & Quataert, E. 2011, *MNRAS*, 413, 2031
- Miceli, M. 2009, *A&A*, 501, 239
- Milne, D. K. 1979, *Aust. J. Phys.*, 32, 83
- Mineo, T. et al. 2001, *A&A*, 380, 695
- Muno, M. P. et al. 2006, *ApJ*, 636, L41
- Ng, C.-Y., Slane, P. O., Gaensler, B. M. & Hughes, J. P. 2008, *ApJ*, 686, 508
- Oskinova, L., M. et al. 2011, *MNRAS*, 416, 1456
- Park, S. et al. 2007, *ApJ*, 670, L121
- Park, S. 2009, *ApJ*, 695, 431
- Park, S. et al. 2012, *ApJ*, 748, 117
- Parmar, A. N., Oostebroek, T., Favata, F., Pightling, S., Coe, M. J., Mereghetti S. & Israel G. l., 1998, *A&A*, 330, 175
- Pavlov, G. G., Sanwal, D., Kiziltan, B. & Garmire, G. P. 2001, *ApJ*, 559, L131
- Pavlov, G. G., Zavlin, V. E., Sanwal, D. & Trümper, J. 2002, *ApJ*, 569, L95
- Pfeffermann, E. & Aschenbach, B. 1996, *International Conference on X-ray Astronomy and Astrophysics: Röntgenstrahlung from the Universe*, 267
- Ray, P. S. et al. 2011, *ApJS*, 194, 17
- Rea, N. , et al. 2010, *Science*, 330, 944
- Rea, N. , et al. 2012, *ApJ*, 754, 27
- Rea, N. & Esposito, P. 2011, *High-Energy Emission from Pulsars and their Systems*, Springer-Verlag Berlin Heidelberg, 247
- Reed, J. E., Hester, J. J., Fabian, A. C. & Winkler, P. F. 1995, *ApJ*, 440, 706
- Reynolds, S. P. et al. 2007, *ApJ*, 668, L135
- Reynoso, E. M., Dubner, G. M., Goss, W. M. & Arnal, E. M. 1995, *AJ*, 110, 318
- Reynoso, E. M. et al. 2004, *PASA*, 21, 82
- Rho, J. H., Petre, R., Schlegel, E. M. & Hester, J. J. 1994, *ApJ*, 430, 757
- Rho, J. H. & Petre, R., 1997, *ApJ*, 484, 828
- Rho, J. H., Petre, R. & Ballet, J., 1998, *Adv. Space Res.*, 22, No 7, 1039
- Ritchie, B. W., Clark, J. S., Negueruela, N. & Langer, N. 2010, *A&A*, 520, A48
- Roger, R. S., Milne, D. K., Kesteven, M. J., Wellington, K. J. & Haynes. R. F. 1988, *ApJ*, 332, 940
- Roy, J., Gupta, Y. & Lewandowski, W. 2012, *MNRAS*, 424, 2213
- Russell, S. C. & Dopita, M. A., 1992, *ApJ*, 384, 508
- Safi-Harb, S. & Oegelman, H. 1994, *AAS*, 184, 5603
- Safi-Harb, S., Oegelman, H. & Finley, J. P. 1995, *ApJ*, 439, 722
- Sanbonmatsu, K. Y. & Helfans, D. J. 1992, *AJ*, 104, 2189
- Sasaki, M., Plucinsky, P.P., Gaetz T.J., Smith, R.K., Edgar R.J. & Slane P.O. 2004, *ApJ*, 617, 322
- Sasaki, M., Plucinsky, P.P., Gaetz T.J. & Bocchino, F. 2013, *A&A*, 552, 45
- Seward, F. D., Slane, P. O., Smith, R. K. & Sun, M. 2003, *ApJ*, 584, 414
- Sezer, A., Gök, F., Hudaverdi M., Aktekin, E. & Ercan, E. N. 2010, *Advances in Hellenic Astronomy during the IYA09, ASP Conf. Series*, 424, 2010
- Slane, P. O., Smith, R. K., Hughes, J. P. & Petre, R. 2002, *ApJ*, 564, 284
- Strom, R. G. & Stappers, B. W. 2000, *ASP Conf. Series, Proceedings of the 177th Col. of the IAU, Bonn (Germany)*, 202, 509
- Strüder, L. et al. 2001, *A&A*, 365, L18
- Su, Y., Chen, Y., Yang, J. et al. 2009, *ApJ*, 694, 376
- Sun, M., Seward, F. D., Smith, R. K. & Slane, P. O. 2004, *ApJ*, 605, 742
- Tam, C. & Roberts, M. S. E. 2003, *ApJ*, 598, L27
- Tamagawa, T. et al. 2009, *PASJ*, 61, S167
- Temim, T., Slane, P., Arendt, R. G. & Dwek, E. 2012, *ApJ*, 745, 46
- Thompson, C. & Duncan, R. C. 1993, *ApJ*, 408, 194
- Thompson, C., Lyutikov M. & Kulkarni, S. R. 2002, *ApJ*, 574, 332
- Tian, W. W. & Leahy, D. A. 2008, *MNRAS*, 391, L54
- Tian, W. W. & Leahy, D. A. 2008, *ApJ*, 677, 292

- Torii, K. et al. 1999, *ApJ*, 523, L69
Torii, K. et al. 2006, *PASJ*, 58, L11
Turner, M. J. L. et al. 2001, *A&A*, 365, L27
Vancura, O., Blare, W. P., Long, K. S. & Raymond, J. C. 1992, *ApJ*, 394, 158
Vasisht, G. & Gotthelf, E. V. 1997, *ApJ*, 486, L129
Vink, J., Bleeker, J., Kaastra, J. S. & Rasmussen, A. 2004, *Nuclear Physics B (Proc. Suppl.)*, 132, 62
Vink, J. & Kuiper, L. 2006, *MNRAS*, 370, L14
Vink, J. 2012, *A&ARv*, 20, 49
Vrba, F. J., Henden, A. A., Luginbuhl, C. B. & Guetter H. H. 2000, *ApJ*, 533, L17
Wang, N., Manchester, R. N., Pace, R. T., Bailes, M., Kaspi, V. M., Stappers, B. W. & Lyne, A. G. 2000, *MNRAS*, 317, 843
Warren, J. S. & Hughes, J. P. 2004, *ApJ*, 608, 261
Weltevrede, P., Johnston, S. & Espinoza, C. M. 2011, *MNRAS*, 411, 1917
Wickramasinghe, D. T. & Ferrario L. 2005, *MNRAS*, 356, 1576
Willingale, R., Bleeker, J. A., van der Heyden, K. J., Kaastra, J. S. & Vink, J. 2002, *A&A*, 381, 1039
Winkler, P. F., Canizares, C. R., Clark, G. W., Markert, T., H. & Petre, R. 1981a, *ApJ*, 245, 574
Winkler, P. F. et al. 1981b, *ApJ*, 246, L27
Winkler, P. F., Twelker, K., Reith, C. N. & Long, K. S. 2009, *ApJ*, 692, 1489
Woltjer, L. 1964, *ApJ*, 140, 1309
Woods, P. M. & Thompson, C. 2006, *Compact Stellar X-ray Sources*, Cambridge Astrophysics Series, 39, 547
Woosley, S. & Janka, T. 2005, *Nature*, 1, 147
Yamaguchi, H. et al. 2008, *PASJ*, 60, S141
Yuan, J. P., Wang, N., Manchester, R. N. & Liu, Z. Y. 2010, *MNRAS*, 404, 289
Zeiger, B. R., Briskin, W. F., Chatterjee, S. & Goss, W. M. 2008, *ApJ*, 674, 271

| Parameter | Kes 73 | CTB 109 | N 49 [†] | Kes 75 |
|------------------------------------------------------------------------------------------|-----------------------------------------|--------------------------------------|-----------------------------------------|--------------------------------------|
| N_H (10^{22}cm^{-2}) | $2.00_{-0.02}^{+0.01}$ | $2.83_{-0.06}^{+0.10}$ | $0.698_{-0.024}^{+0.006}$ | $1.79_{-0.05}^{+0.06}$ |
| kT_1 (keV) | $0.43_{-0.05}^{+0.02}$ | $0.065_{-0.002}^{+0.001}$ | $0.230_{-0.003}^{+0.004}$ | $2.8_{-0.1}^{+0.2}$ |
| N_1^{brems} (Norm. counts s^{-1}) | $0.36_{-0.02}^{+0.15}$ | $9_{-14}^{+1} \times 10^6$ | $0.512_{-0.007}^{+0.067}$ | $(4.5_{-0.3}^{+0.2}) \times 10^{-3}$ |
| kT_2 (keV) | $1.34_{-0.01}^{+0.01}$ | $0.20_{-0.02}^{+0.03}$ | $1.14_{-0.01}^{+0.04}$ | - |
| N_2^{brems} (Norm. counts s^{-1}) | $(2.47_{-0.06}^{+0.41}) \times 10^{-2}$ | 18_{-4}^{+9} | $(3.5_{-0.15}^{+0.08}) \times 10^{-3}$ | - |
| N VII (3,4 \rightarrow 1) | | | | |
| E (keV) | - | $0.515_{-0.008}^{+0.016}$ | - | - |
| σ (keV) | - | $9.2_{-0.3}^{+0.1} \times 10^{-2}$ | - | - |
| N (Norm. counts s^{-1}) | - | $(4_{-1}^{+1}) \times 10^4$ | - | - |
| EW^{\ddagger} (eV) | - | 737 | - | - |
| O VII (2,5 \rightarrow 1) | | | | |
| E (keV) | - | - | $0.568_{-0.004}^{+0.004}$ | - |
| σ (keV) | - | - | $(6.1_{-0.3}^{+0.1}) \times 10^{-2}$ | - |
| N (Norm. counts s^{-1}) | - | - | $(4.7_{-0.3}^{+0.7}) \times 10^{-2}$ | - |
| EW^{\ddagger} (eV) | - | - | 198 | - |
| N VII (6,7 \rightarrow 1)/O VII (2,5,6 \rightarrow 1) | | | | |
| E (keV) | - | $0.597_{-0.002}^{+0.003}$ | - | - |
| σ (keV) | - | < 0.06 | - | - |
| N (Norm. counts s^{-1}) | - | $(2.4_{-0.4}^{+1.5}) \times 10^5$ | - | - |
| EW^{\ddagger} (eV) | - | 472 | - | - |
| O VIII (6,7 \rightarrow 1)/Fe XVIII (4,5 \rightarrow 1) | | | | |
| E (keV) | - | - | $0.769_{-0.001}^{+0.001}$ | - |
| σ (keV) | - | - | $0.112_{-0.003}^{+0.002}$ | - |
| N (Norm. counts s^{-1}) | - | - | $(1.78_{-0.06}^{+0.11}) \times 10^{-2}$ | - |
| EW^{\ddagger} (eV) | - | - | 338 | - |
| Ne IX (2,5 \rightarrow 1) | | | | |
| E (keV) | - | $0.91_{-0.01}^{+0.01}$ | - | - |
| σ (keV) | - | < 0.07 | - | - |
| N (Norm. counts s^{-1}) | - | $7.2_{-0.6}^{+0.2}$ | - | - |
| EW^{\ddagger} (eV) | - | 147 | - | - |
| Ne X (3,4 \rightarrow 1) | | | | |
| E (keV) | - | $1.014_{-0.003}^{+0.002}$ | $1.028_{-0.001}^{+0.004}$ | - |
| σ (keV) | - | < 0.07 | < 0.07 | - |
| N (Norm. counts s^{-1}) | - | $0.37_{-0.04}^{+0.03}$ | $(5.9_{-0.3}^{+0.3}) \times 10^{-4}$ | - |
| EW^{\ddagger} (eV) | - | 68 | 33 | - |
| Mg XI (2 \rightarrow 1) | | | | |
| E (keV) | $1.346_{-0.002}^{+0.001}$ | $1.347_{-0.004}^{+0.003}$ | $1.332_{-0.002}^{+0.006}$ | $1.33_{-0.02}^{+0.02}$ |
| σ (keV) | < 0.08 | < 0.08 | < 0.08 | < 0.08 |
| N (Norm. counts s^{-1}) | $2.6_{-0.1}^{+0.1} \times 10^{-3}$ | $(2.0_{-0.1}^{+0.3}) \times 10^{-3}$ | $(2.03_{-0.08}^{+0.08}) \times 10^{-4}$ | $(1.8_{-0.3}^{+0.3}) \times 10^{-4}$ |
| EW^{\ddagger} (eV) | 95 | 337 | 62 | 84 |

[†] The absorption column density of N49 is fitted using the LMC abundances: He=0.89, C=0.30, N=0.12, O=0.26, Ne=0.33, Na=0.30, Mg=0.32, Al=0.30, Si=0.30, S=0.31, Cl=0.31, Ar=0.54, Ca=0.34, Cr=0.61, Fe=0.36, Co=0.30 & Ni=0.62. We have added also the galactic absorption $N_H = 6 \times 10^{20} \text{cm}^{-2}$.

[‡] Equivalent Width.

Table 3. Summary of the fitted models for Kes 73, CTB 109, N 49 and Kes 75.

| Parameter | Kes 73 | CTB 109 | N 49 [†] | Kes 75 |
|-------------------------------------|---------------------------------------|--------------------------------------|-----------------------------------------|-----------------------------------------|
| Mg XII (3,4 → 1) | | | | |
| E (keV) | - | - | $1.459_{+0.006}^{-0.005}$ | - |
| σ (keV) | - | - | < 0.08 | - |
| N (Norm. counts s ⁻¹) | - | - | $(3.9_{+0.6}^{-0.5}) \times 10^{-5}$ | - |
| EW^{\ddagger} (eV) | - | - | 20 | - |
| Si XIII (2,5,6,7 → 1) | | | | |
| E (keV) | $1.8521_{+0.0001}^{-0.0001}$ | $1.856_{+0.006}^{-0.001}$ | $1.848_{+0.002}^{-0.003}$ | $1.851_{+0.012}^{-0.003}$ |
| σ (keV) | < 0.02 | < 0.02 | $(2.3_{+0.6}^{-0.6}) \times 10^{-2}$ | < 0.02 |
| N (Norm. counts s ⁻¹) | $2.76_{+0.06}^{-0.06} \times 10^{-3}$ | $(7.0_{+0.3}^{-0.2}) \times 10^{-4}$ | $(1.68_{+0.06}^{-0.04}) \times 10^{-4}$ | $(2.6_{+0.2}^{-0.1}) \times 10^{-4}$ |
| EW^{\ddagger} (eV) | 368 | 278 | 299 | 232 |
| Si XIV (3,4 → 1) | | | | |
| E (keV) | - | - | $1.998_{+0.007}^{-0.002}$ | - |
| σ (keV) | - | - | < 0.09 | - |
| N (Norm. counts s ⁻¹) | - | - | $(5.2_{+0.3}^{-0.4}) \times 10^{-5}$ | - |
| EW^{\ddagger} (eV) | - | - | 132 | - |
| Si XIII (13 → 1) | | | | |
| E (keV) | $2.201_{+0.009}^{-0.010}$ | - | - | $2.21_{+0.04}^{-0.02}$ |
| σ (keV) | < 0.09 | - | - | < 0.09 |
| N (Norm. counts s ⁻¹) | $(1.6_{+0.2}^{-0.2}) \times 10^{-4}$ | - | - | $(3.4_{+1.1}^{-0.9}) \times 10^{-5}$ |
| EW^{\ddagger} (eV) | 46 | - | - | 45 |
| S XV (2,5,6,7 → 1) | | | | |
| E (keV) | $2.452_{+0.002}^{-0.002}$ | - | $2.444_{+0.005}^{-0.005}$ | $2.437_{+0.007}^{-0.005}$ |
| σ (keV) | < 0.09 | - | < 0.09 | < 0.09 |
| N (Norm. counts s ⁻¹) | $(8.0_{+0.2}^{-0.3}) \times 10^{-4}$ | - | $(6.8_{+0.4}^{-0.4}) \times 10^{-5}$ | $(1.09_{+0.08}^{-0.12}) \times 10^{-4}$ |
| EW^{\ddagger} (eV) | 375 | - | 299 | 178 |
| S XV (13 → 1) | | | | |
| E (keV) | - | - | - | - |
| σ (keV) | - | - | - | - |
| N (Norm. counts s ⁻¹) | - | - | - | - |
| EW^{\ddagger} (eV) | - | - | - | - |
| Ar XVII (2,5,6,7 → 1) | | | | |
| E (keV) | $3.13_{+0.01}^{-0.01}$ | - | $3.12_{+0.02}^{-0.02}$ | - |
| σ (keV) | < 0.1 | - | < 0.1 | - |
| N (Norm. counts s ⁻¹) | $(9_{+1}^{-1}) \times 10^{-5}$ | - | $(7_{+1}^{-1}) \times 10^{-6}$ | - |
| EW^{\ddagger} (eV) | 120 | - | 110 | - |
| Fe XXV (7 → 1) | | | | |
| E (keV) | $6.7_{+0.2}^{-0.2}$ | - | - | - |
| σ (keV) | $0.5_{+0.2}^{-0.1}$ | - | - | - |
| N (Norm. counts s ⁻¹) | $2.9_{+0.6}^{-0.6} \times 10^{-5}$ | - | - | - |
| EW^{\ddagger} (eV) | 1890 | - | - | - |
| χ_r^2 | 1.57 (985) | 2.05 (477) | 1.84 (578) | 1.12 (258) |

[†] The absorption column density of N49 is fitted using the LMC abundances: He=0.89, C=0.30, N=0.12, O=0.26, Ne=0.33, Na=0.30, Mg=0.32, Al=0.30, Si=0.30, S=0.31, Cl=0.31, Ar=0.54, Ca=0.34, Cr=0.61, Fe=0.36, Co=0.30 & Ni=0.62. We have added also the galactic absorption $N_H = 6 \times 10^{20} \text{ cm}^{-2}$.

[‡] Equivalent Width.

Table 4. Continued.

| Parameter | VNEI | | | |
|---------------------------------------------|-----------------------------------------------------------|-----------------------------------------------------------|----------------------------------------------------------------|-----------------------------------------------------------|
| | Kes 73 | CTB 109 | N 49 [†] | Kes 75 |
| N_H (cm ⁻²) | 2.51 ^{-0.08} _{+0.06} | 0.695 ^{-0.018} _{+0.005} | 1.03 ^{-0.02} _{+0.02} | 3.71 ^{-0.06} _{+0.07} |
| kT_{brems} (keV) | 0.41 ^{+0.05} _{+0.03} | - | 0.95 ^{+0.02} _{+0.01} | 0.31 ^{+0.05} _{+0.04} |
| N_{brems} (Norm. counts s ⁻¹) | 0.5 ^{-0.2} _{+0.2} | - | (5.4 ^{-0.3} _{+0.3}) × 10 ⁻³ | 0.4 ^{-0.2} _{+0.5} |
| kT (keV) | 1.51 ^{-0.08} _{+0.15} | 0.297 ^{-0.004} _{+0.007} | 0.1650 ^{-0.0003} _{+0.0011} | 2.0 ^{-0.1} _{+0.2} |
| O | 1 (fixed) | 0.16 ^{-0.02} _{+0.01} | 0.137 ^{-0.003} _{+0.002} | 1 (fixed) |
| Ne | 1 (fixed) | 0.27 ^{-0.01} _{+0.01} | 0.175 ^{-0.004} _{+0.004} | 1 (fixed) |
| Mg | 1.30 ^{-0.11} _{+0.09} | 0.23 ^{-0.02} _{+0.01} | 0.36 ^{-0.01} _{+0.01} | 0.51 ^{-0.08} _{+0.09} |
| Si | 1.6 ^{-0.2} _{+0.1} | 0.49 ^{-0.05} _{+0.03} | 1 (fixed) | 0.56 ^{-0.04} _{+0.05} |
| S | 2.1 ^{-0.2} _{+0.4} | 1 (fixed) | 1 (fixed) | 0.9 ^{-0.1} _{+0.2} |
| Ar | 3.1 ^{-0.6} _{+0.9} | 1 (fixed) | 1 (fixed) | 1.2 ^{-0.6} _{+0.8} |
| Ca | 6 ⁻² ₊₄ | 1 (fixed) | 1 (fixed) | 1 (fixed) |
| Fe | 1 (fixed) | 0.226 ^{-0.024} _{+0.008} | 1 (fixed) | 1 (fixed) |
| E_1 (keV) | - | - | 0.729 ^{-0.002} _{+0.005} | - |
| σ_1 (keV) | - | - | < 0.07 | - |
| N_1 (Norm. counts s ⁻¹) | - | - | (5.4 ^{-0.3} _{+0.3}) × 10 ⁻³ | - |
| E_2 (keV) | - | - | 1.018 ^{-0.001} _{+0.001} | - |
| σ_2 (keV) | - | - | < 0.07 | - |
| N_2 (Norm. counts s ⁻¹) | - | - | (1.200 ^{-0.04} _{+0.008}) × 10 ⁻³ | - |
| E_3 (keV) | - | - | 1.467 ^{-0.004} _{+0.004} | - |
| σ_3 (keV) | - | - | < 0.08 | - |
| N_3 (Norm. counts s ⁻¹) | - | - | (4.9 ^{-0.6} _{+0.6}) × 10 ⁻⁵ | - |
| E_4 (keV) | - | - | 1.846 ^{-0.003} _{+0.003} | - |
| σ_4 (keV) | - | - | < 0.09 | - |
| N_4 (Norm. counts s ⁻¹) | - | - | (1.56 ^{-0.07} _{+0.07}) × 10 ⁻⁴ | - |
| E_5 (keV) | - | - | 1.998 ^{-0.003} _{+0.028} | - |
| σ_5 (keV) | - | - | < 0.09 | - |
| N_5 (Norm. counts s ⁻¹) | - | - | (5.3 ^{-0.5} _{+0.5}) × 10 ⁻⁵ | - |
| E_6 (keV) | - | - | 2.445 ^{-0.005} _{+0.005} | - |
| σ_6 (keV) | - | - | < 0.1 | - |
| N_6 (Norm. counts s ⁻¹) | - | - | (6.4 ^{-0.4} _{+0.3}) × 10 ⁻⁵ | - |
| E_7 (keV) | - | - | 3.12 ^{-0.02} _{+0.02} | - |
| σ_7 (keV) | - | - | < 0.1 | - |
| N_7 (Norm. counts s ⁻¹) | - | - | (7 ⁻¹ ₊₁) × 10 ⁻⁶ | - |
| τ (s cm ⁻³) | (5.1 ^{-0.8} _{+0.6}) × 10 ¹⁰ | (6.7 ^{-1.0} _{+0.8}) × 10 ¹¹ | (1.3 ^{-0.2} _{+0.1}) × 10 ¹² | (2.4 ^{-0.3} _{+0.3}) × 10 ¹⁰ |
| N (Norm. counts s ⁻¹) | (3.9 ^{-0.9} _{+0.6}) × 10 ⁻² | 0.35 ^{-0.04} _{+0.02} | 1.69 ^{-0.02} _{+0.03} | 0.021 ^{-0.003} _{+0.003} |
| χ_r^2 | 1.56 (997) | 2.60 (491) | 1.87 (569) | 1.19 (236) |

Table 5. Fits for Kes 73, CTB 109, N 49 & Kes 75 using a `vnei` plasma model. A second thermal Bremsstrahlung component is included in some cases.[†] The absorption column density of N49 is fitted using the LMC abundances: He=0.89, C=0.30, N=0.12, O=0.26, Ne=0.33, Na=0.30, Mg=0.32, Al=0.30, Si=0.30, S=0.31, Cl=0.31, Ar=0.54, Ca=0.34, Cr=0.61, Fe=0.36, Co=0.30 & Ni=0.62. We have added also the galactic absorption $N_H = 6 \times 10^{20} \text{ cm}^{-2}$.

| SNRs with magnetars | | | | | | | | |
|-----------------------|-----------------------|--------------------------------|---------------------------|-----------------------------|----------------------------------|----------------------------|-----------------------------------------------|--------------------------------------------|
| Name | Central source | Distance (kpc) | Radius (pc) | Age (kyr) | \dot{E} (erg s ⁻¹) | B_s (G) | F_X (erg cm ⁻² s ⁻¹) | L_X (erg s ⁻¹) |
| Kes 75 | J1846-0258 [26] | 10.6 [66] | $5.5_{+0.3}^{-0.3}$ [10] | 0.9 [6] | 8.06×10^{36} [40] | 4.88×10^{13} [40] | 2.69×10^{-10} | 3.61×10^{36} |
| Kes 73 | 1E 1841-045 [72] | $6.7_{+1.8}^{-1.0}$ [61] | $4.5_{+0.1}^{-0.1}$ [10] | $1.3_{+0.2}^{-0.2}$ [73] | 1.08×10^{33} [31] | 7.34×10^{14} [31] | 4.39×10^{-10} | $2.36_{+1.43}^{-0.65} \times 10^{36}$ |
| N 49 | RX J0526-6604 [36] | 50 [36] | $20.4_{+0.8}^{-1.0}$ [10] | 4.8 [48] | 4.92×10^{33} [36] | 7.32×10^{14} [36] | 2.41×10^{-10} | 7.21×10^{37} |
| CTB 109 | 1E 2259+586 [2] | $3_{+0.5}^{-0.5}$ [33] | $12.6_{+1.3}^{-1.3}$ [10] | 14_{+2}^{-2} [62] | 5.54×10^{31} [2] | 5.84×10^{13} [2] | 1.94×10^{-10} | $2.09_{+0.75}^{-0.64} \times 10^{35}$ |
| SNRs with CCOs | | | | | | | | |
| Cas A | CXO J2323+5848 [45] | $3.4_{+0.3}^{-0.1}$ [53] | $2.8_{+0.1}^{-0.1}$ [10] | 0.326_{+27}^{-27} [17] | - | - | 2.06×10^{-8} [10] | $2.85_{+0.50}^{-0.20} \times 10^{37}$ [10] |
| G350.1-0.3 | XMMU J1720-3726 [23] | 4.5 [23] | $2.5_{+0.4}^{-0.1}$ [10] | 0.9 [23] | - | - | 1.64×10^{-9} [10] | 3.97×10^{36} [10] |
| G330.2+1.0 | CXOU J1601-5133 [47] | $4.9_{+0.3}^{-0.3}$ [53] | $7.8_{+0.8}^{-0.8}$ [10] | 1.1 [47] | - | - | 1.60×10^{-11} [71] | $4.60_{+0.57}^{-0.55} \times 10^{34}$ [71] |
| G347.3-0.5 | 1 WGA J1713-3949 [38] | 1 [34] | $8.7_{+0.8}^{-0.8}$ [18] | 1.6 [18] | - | - | 4.40×10^{-10} [51] | 5.26×10^{34} |
| Vela Jr. | CXOU J0852-4617 [49] | $0.75_{+0.25}^{-0.55}$ [31] | 13.1 [10] | $1.7_{+2.6}^{-0}$ [31] | - | - | 8.30×10^{-11} [1] | $5.58_{+4.34}^{-3.10} \times 10^{33}$ |
| RCW 103 | 1E 1613-5055 [25] | 3.1 [55] | $4.1_{+0.1}^{-0.1}$ [10] | 2 [7] | - | - | 1.70×10^{-8} [10] | 1.95×10^{37} |
| G349.7+0.2 | CXOU J1718-3726 [39] | 22.4 [20] | 8.2 [39] | 3.5 [39] | - | - | 6.50×10^{-10} [39] | 3.90×10^{37} |
| Puppis A | RX J0822-4300 [4] | $2.2_{+0.3}^{-0.3}$ [54] | $17.5_{+1.7}^{-1.7}$ [16] | $4.45_{+0.75}^{-0.75}$ [4] | - | - | 2.16×10^{-8} | $1.20_{+1.55}^{0.90} \times 10^{37}$ [14] |
| Kes 79 | J1852+0040 [63] | 7.1 [8] | $9.2_{+1.0}^{-1.0}$ [10] | $6.0_{+0.4}^{-0.2}$ [67] | 2.96×10^{32} [27] | 3.05×10^{10} [27] | 4.64×10^{-10} [67] | 2.80×10^{36} [67] |
| G296.5+10.0 | 1E 1207-5209 [24] | $2.1_{+1.8}^{-0.8}$ [24] | 24.8 [32] | 7 [57] | 9.58×10^{33} [50] | 2.83×10^{12} [50] | 1.67×10^{-9} [44] | $8.81_{+21.60}^{-5.40} \times 10^{34}$ |
| SNRs with high-B PSRs | | | | | | | | |
| MSH 15-52 | J1513-5908 [21] | $5.2_{+1.4}^{-1.4}$ [15] | 22.7 [46] | 1.9 [15] | 1.75×10^{37} [41] | 1.54×10^{13} [41] | 7.80×10^{-11} [46] | $2.52_{+1.54}^{-1.17} \times 10^{35}$ |
| MSH 11-54 | J1124-5916 [29] | $6.2_{+0.9}^{-0.9}$ [22] | $16.2_{+0.2}^{-0.2}$ [10] | $2.99_{+0.06}^{-0.06}$ [76] | 1.19×10^{37} [52] | 1.02×10^{13} [52] | 2.09×10^{-9} [10] | $9.61_{+2.99}^{-2.59} \times 10^{36}$ |
| G292.2-0.5 | J1119-6127 [37] | $8.4_{+0.4}^{-0.4}$ [9] | $21.1_{+3.8}^{-3.8}$ [10] | $7.1_{+0.5}^{-0.2}$ [37] | 2.34×10^{36} [75] | 4.10×10^{13} [75] | 1.98×10^{-11} [37] | $1.67_{+0.16}^{-0.13} \times 10^{35}$ |
| SNRs with normal PSRs | | | | | | | | |
| G21.5-0.9 | J1833-1034 [43] | $4.7_{+0.4}^{-0.4}$ [69] | $3.2_{+0.1}^{-0.1}$ [10] | $0.87_{+2.0}^{-1.5}$ [5] | 3.37×10^{37} [58] | 3.58×10^{12} [58] | 6.69×10^{-13} | $1.77_{+0.29}^{-0.31} \times 10^{33}$ [43] |
| G11.2-0.3 | J1811-1925 [70] | 5 [30] | $2.3_{+0.1}^{-0.1}$ [10] | 1.616 [68] | 6.42×10^{36} [70] | 1.71×10^{12} [70] | 3.98×10^{-9} [10] | 1.19×10^{37} [10] |
| G8.7-0.1 | J1803-2137 [19] | 4 [19] | 29.1 [19] | 15_{+6}^{-6} [19] | 2.22×10^{36} [77] | 4.92×10^{12} [77] | 2.00×10^{-10} [19] | 3.83×10^{35} |
| Vela | J0835-4510 [3] | $0.287_{+0.019}^{-0.017}$ [13] | 20.1 [42] | 18_{+9}^{-9} [3] | 6.92×10^{36} [12] | 3.38×10^{12} [12] | 2.94×10^{-8} | $2.90_{+0.39}^{-1.34} \times 10^{35}$ [42] |
| MSH 11-61A | J1105-6107 [64] | 7 [64] | $12.1_{+2.2}^{-2.2}$ [64] | 20_{+5}^{-5} [64] | 2.48×10^{36} [74] | 1.01×10^{12} [74] | 8.06×10^{-11} [10] | 4.71×10^{35} [10] |
| W 44 | J1856+0113 [11] | 2.5 [11] | $10.8_{+2.0}^{-2.0}$ [11] | 20_{+4}^{-4} [11] | 4.30×10^{35} [28] | 7.55×10^{12} [28] | 1.80×10^{-9} [56] | 1.35×10^{36} |
| CTB 80 | J1952+3252 [60] | 2 [65] | 1.5 [60] | 51 [78] | 3.74×10^{36} [28] | 4.86×10^{11} [28] | 2.40×10^{-12} | 1.15×10^{33} [59] |

Table 6. SNRs considered in our X-ray luminosity analysis. The data without references is extracted from this work or deduced from the data obtained in the literature. The references are: [1]Aharonian et al. (2007), [2]Archibald et al. (2013), [3]Aschbacher et al. (1995), [4]Becker et al. (2012), [5]Bietenholz & Bartel (2008), [6]Blanton & Helfand (1996), [7]Carter et al. (1997), [8]Case & Bhattacharya (1998), [9]Caswell et al. (2004), [10]Chandra SNR catalog⁴, [11]Cox et al. (1999), [12]Dodson et al. (2002), [13]Dodson et al. (2003), [14]Dubner et al. (2013), [15]Fang & Zhang (2010), [16]Ferrand & Safi-Harb (2012), [17]Fesen et al. (2006), [18]Fesen et al. (2012), [19]Finley & Oegelman (1994), [20]Frail et al. (1996), [21]Gaensler et al. (1999), [22]Gaensler & Wallace (2003), [23]Gaensler et al. (2008), [24]Giacani et al. (2000), [25]Gotthelf et al. (1999a), [26]Gotthelf et al. (2000), [27]Halpern & Gotthelf (2010), [28]Hobbs et al. (2004), [29]Hughes et al. (2003), [30]Kaspi et al. (2001), [31]Katsuda et al. (2008), [32]Kellett et al. (1987), [33]Kothes et al. (2002), [34]Koyama et al. (1997), [35]Kuiper et al. (2006), [36]Kulkarni et al. (2003), [37]Kumar et al. (2012), [38]Lazendic et al. (2003), [39]Lazendic et al. (2005), [40]Livingstone et al. (2011a), [41]Livingstone & Kaspi (2011b), [42]Lu & Aschenbach (2000), [43]Matheson & Safi-Harb (2010), [44]Matsui et al. (1988), [45]Mereghetti et al. (2002), [46]Mineo et al. (2001), [47]Park et al. (2009), [48]Park et al. (2012), [49]Pavlov et al. (2001), [50]Pavlov et al. (2002), [51]Pfeffermann & Aschenbach (1996), [52]Ray et al. (2011), [53]Reed et al. (1995), [54]Reynoso et al. (1995), [55]Reynoso et al. (2004), [56]Rho et al. (1994), [57]Roger et al. (1988), [58]Roy et al. (2012), [59]Safi-Harb & Oegelman (1994), [60]Safi-Harb et al. (1995), [61]Sanbonmatsu & Helfand (1992), [62]Sasaki et al. (2013), [63]Seward et al. (2003), [64]Slane et al. (2002), [65]Strom & Stappers (2000), [66]Su et al. (2009), [67]Sun et al. (2004), [68]Tam & Roberts (2003), [69]Tian & Leahy (2008a), [70]Torii et al. (1999), [71]Torii et al. (2006), [72]Vasisht & Gotthelf (1997), [73]Vink & Kuiper (2006), [74]Wang et al. (2000), [75]Weltevrede et al. (2011), [76]Winkler et al. (2009), [77]Yuan et al. (2010), [78]Zeiger et al. (2008).

| SNR | Galaxy | Age (yr) | Element | | | | | |
|------------------------|--------|-----------|-----------------------------|-----------------------------|-----------------------------|------------------------------|--------------------------|-----------------------------|
| | | | <i>O VII</i> | <i>O VIII</i> | <i>O VIII</i> | <i>Ne IX</i> | <i>Ne X</i> | <i>Ne X</i> |
| | | | (2,5,7 → 1) (0.574 KeV) | (3,4 → 1) (0.653 KeV) | (6,7 → 1) (0.774 KeV) | (2,5 → 1) (0.915 KeV) | (3,4 → 1) (1.022 KeV) | (6,7 → 1) (1.21 KeV) |
| Kes73 | MW | 1100-1500 | | | | | | |
| CTB109 | MW | 7900-9700 | | | | X | X | |
| Kes75 | MW | 900-4300 | | | | | | |
| N49 | LMC | 5000 | X | | X | X | X | |
| G1.9+1.3 [2] | MW | 110-170 | | | | | | |
| Kepler [3],[8],[12] | MW | 408 | | | | X | | |
| Tycho [4],[5],[6],[13] | MW | 440 | | | | X | | |
| SN1006 [10],[19] | MW | 1006 | X | | X | | | X |
| Cas A [1],[9],[16] | MW | 316-352 | X | X | X | | X | |
| MSH11-54 [11],[14] | MW | 2930-3050 | X | X | X | X | X | |
| Puppis A [7],[17],[18] | MW | 3700-5500 | X | X | X | X | X | X |
| B0509-67.5 [15] | LMC | 400 | X | X | | X | | |
| | | | <i>Mg XI</i> | <i>Mg XII</i> | <i>Si XIII</i> | <i>Si XIV</i> | <i>Si XIII</i> | <i>S XV</i> |
| | | | (2,5,6,7 → 1) (1.35 KeV) | (3,4 → 1) (1.47 KeV) | (2,5,6,7 → 1) (1.86 KeV) | (3,4 → 1) (2.00 KeV) | (13 → 1) (2.18 KeV) | (2,5,6,7 → 1) (2.46 KeV) |
| Kes73 | MW | 1100-1500 | X | | X | | X | X |
| CTB109 | MW | 7900-9700 | X | | X | | | |
| Kes75 | MW | 900-4300 | X | | X | | X | X |
| N49 | LMC | 5000 | X | X | X | X | | X |
| G1.9+1.3 | MW | 110-170 | X | | X | | | X |
| Kepler | MW | 408 | X | | X | X | X | X |
| Tycho | MW | 440 | | | X | X | X | X |
| SN1006 | MW | 1006 | X | | X | | | |
| Cas A | MW | 316-352 | X | X | X | X | X | X |
| MSH11-54 | MW | 2930-3050 | X | X | X | | | X |
| Puppis A | MW | 3700-5500 | X | | X | | X | X |
| B0509-67.5 | LMC | 400 | X | | X | | X | X |
| | | | <i>S XV</i> | <i>Ar XVII</i> | <i>Ca XIX</i> | <i>Fe XXV</i> | <i>K-shell</i> | |
| | | | (13 → 1) (2.88 KeV) | (2,5,6,7 → 1) (3.13 KeV) | (2,5,6,7 → 1) (3.89 KeV) | <i>K-shell</i> (6.65 KeV) | | |
| Kes73 | MW | 1100-1500 | | X | | X | | |
| CTB109 | MW | 7900-9700 | | | | | | |
| Kes75 | MW | 900-4300 | | | | | | |
| N49 | LMC | 5000 | | X | | | | |
| G1.9+1.3 | MW | 110-170 | | X | X | X | | |
| Kepler | MW | 408 | X | X | X | X | | |
| Tycho | MW | 440 | X | X | X | X | | |
| SN1006 | MW | 1006 | | | | | | |
| Cas A | MW | 316-352 | X | X | X | X | | |
| MSH11-54 | MW | 2930-3050 | | | | | | |
| Puppis A | MW | 3700-5500 | | | | | | |
| B0509-67.5 | LMC | 400 | | X | X | X | | |

Table 7. Summary of line detections in X-ray for some important SNRs compared with lines detected in our analysis. The references are: ^[1]Bleeker et al. (2001), ^[2]Borkowski et al. (2010), ^[3]Cassam-Chenaï et al. (2004), ^[4]Decourchelle et al. (2001), ^[5]Hayato et al. (2010), ^[6]Hwang & Gotthelf (1997), ^[7]Hwang et al. (2008), ^[8]Kinugasa & Tsunemi (1987), ^[9]Maeda et al. (2009), ^[10]Miceli et al. (2009), ^[11]Park et al. (2007), ^[12]Reynolds et al. (2007), ^[13]Tamagawa et al. (2009), ^[14]Vink et al. (2004), ^[15]Warren & Hughes (2004), ^[16]Willingale et al. (2002), ^[17]Winkler et al. (1981a), ^[18]Winkler et al. (1981b), ^[19]Yamaguchi et al. (2008)